J Comput Aided Mol Des (2013) 27:247–256
DOI 10.1007/s10822-012-9630-6

A quantum mechanics/molecular mechanics study on the hydrolysis mechanism of New Delhi metallo-β-lactamase-1

Kongkai Zhu · Junyan Lu · Zhongjie Liang · Xiangqian Kong · Fei Ye · Lu Jin · Heji Geng · Yong Chen · Mingyue Zheng · Hualiang Jiang · Jun-Qian Li · Cheng Luo

Received: 14 October 2012 / Accepted: 28 December 2012 / Published online: 2 March 2013

Abstract New Delhi metallo-β-lactamase-1 (NDM-1) has emerged as a major global threat to human health for its rapid rate of dissemination and ability to make pathogenic microbes resistant to almost all known β-lactam antibiotics. In addition, effective NDM-1 inhibitors have not been identified to date. In spite of the plethora of structural and kinetic data available, the accurate molecular characteristics of and details on the enzymatic reaction of NDM-1 hydrolyzing β-lactam antibiotics remain incompletely understood. In this study, a combined computational approach including molecular docking, molecular dynamics simulations and quantum mechanics/molecular mechanics calculations was performed to characterize the catalytic mechanism of meropenem catalyzed by NDM-1. The quantum mechanics/molecular mechanics results indicate that the ionized D124 is beneficial to the cleavage of the C–N bond within the β-lactam ring. Meanwhile, it is energetically favorable to form an intermediate if no water molecule coordinates to Zn2. Moreover, according to the molecular dynamics results, the conserved residue K211 plays a pivotal role in substrate binding and catalysis, which is quite consistent with previous mutagenesis data. Our study provides detailed insights into the catalytic mechanism of NDM-1 hydrolyzing meropenem β-lactam antibiotics and offers clues for the discovery of new antibiotics against NDM-1 positive strains in clinical studies.

Keywords QM/MM · NDM-1 · MD · Catalytic mechanism · β-Lactam antibiotics

Abbreviations

NDM-1	New Delhi metallo-β-lactamase-1
MBLs	Metallo-β-lactamases
MD	Molecular dynamics
QM/MM	Quantum mechanics/molecular mechanics
RMSD	Root mean square deviation

Introduction

β-Lactam containing compounds are the most widely used antibiotics for the treatment of severe bacterial infections. They are inexpensive and exhibit their bactericidal activity by inhibiting the transpeptidase involved in bacterial cell wall synthesis [1]. Unfortunately, the emergence of β-lactamase-mediated resistance to β-lactam antibiotics has become a major clinical and epidemiological concern as β-lactamases are capable of cleaving the C–N bond within the β-lactam ring to render the antibiotics inactive. There are four classes of β-lactamases [2], namely, classes A–D. Classes A, C, and D enzymes belong to the family of serine β-lactamases, whereas class B lactamases are characterized

Kongkai Zhu and Junyan Lu contributed equally to this work.

Electronic supplementary material The online version of this article (doi:10.1007/s10822-012-9630-6) contains supplementary material, which is available to authorized users.

K. Zhu · H. Geng · Y. Chen (✉) · J.-Q. Li
Department of Chemistry, Fuzhou University, Fujian 350108, China
e-mail: heishh@fzu.edu.cn

K. Zhu · J. Lu · X. Kong · F. Ye · L. Jin · H. Geng · M. Zheng · H. Jiang · C. Luo (✉)
State Key Laboratory of Drug Research, Shanghai Institute of Materia Medica, Chinese Academy of Sciences, 555 Zuchongzhi Road, Shanghai 201203, China
e-mail: cluo@mail.shcnc.ac.cn

Z. Liang · C. Luo
Center for Systems Biology, Soochow University, Jiangsu 215006, China

by one or two zinc ions located in their active site and usually termed metallo-β-lactamases (MBLs) [3–5]. Based on their amino acid sequence homology and zinc ion dependence, MBLs have been further classified into three subclasses: B1, B2, and B3 [2–6]. MBLs have drawn increasing attentions, for their rapid dissemination, extreme substrate diversity, and ability to hydrolyze "last resort" carbapenem antibiotics [7]. In addition, inhibitors that could inactivate serine β-lactamases are ineffective against MBLs. Up to now, clinically useful inhibitors of MBLs have not been identified [8].

New Delhi metallo-β-lactamase-1 (NDM-1) is a broad spectrum plasmid-encoded β-lactamase first identified from *Klebsiella pneumonia* isolated in Sweden in 2008 from a patient who had travelled to New Delhi [9]. As is the case for MBLs, *K. pneumonia* NDM-1-positive or *Escherichia coli* NDM-1-positive strains can hydrolyze almost all antibiotics, including penicillins, cephalosporins, and the highly potent carbapenems, except tigecycline and colistin [10]. In addition, most plasmids that harbor the NDM-1 gene often co-harbor a large number of other resistance genes, such as those for quinolones, aminoglycosides, rifampin, sulfonamides, and macrolides [11–13], which makes NDM-1-positive strain resistance to multiple drugs. The rapid and extensive spread of NDM-1-positive strains has been stressed in many reports since 2010 [10, 14–16]. Moreover, there are no effective inhibitors of NDM-1, and its catalytic mechanism remains elusive. Taken together, these results indicate that NDM-1 has become a serious threat to human health.

Considerable efforts have been made to characterize the structure of NDM-1, and now there are nine crystal structures of the enzyme available in the Protein Data Bank (PDB) [17–21]. The active site contains two zinc ions, Zn1 is coordinated to three histidine residues (H120, H122 and H189) and a bridging hydroxide ion, whereas Zn2 has five ligands, namely, an aspartate (D124), a cysteine (C208), a histidine (H250), apical water (WAT), and a bridging hydroxide ion. Based on its amino acid sequence homology and active site residues, NDM-1 has been categorized under the B1 MBL subclass [10].

Although much effort has been devoted to understanding the structural properties of NDM-1, its catalytic mechanism has not been elucidated yet. However, a considerable number of studies have been carried out to understand the binding and catalytic properties of other MBLs through experimental and theoretical approaches [22–33]. According to these studies, there are two principal viewpoints about the catalytic mechanism of di-zinc MBLs. These two main catalytic mechanisms differ in the substrate binding mode. While Dal Peraro et al. assumed that the carboxyl group, which is conserved in β-lactam antibiotics, interacted with Zn2 indirectly through the water molecule chelated with Zn2, Park et al. proposed that the substrate was bond in the active site through direct coordination of substrate carboxyl group to Zn2.

In this study, four enzyme–substrate (ES) complex models (models A–D) that differ in the protonation state of the D124 residue and in the presence or absence of liganded water in Zn2 were constructed. Molecular dynamics (MD) simulations were performed on these ES complexes. After 30-ns MD simulations for each complex, a quantum mechanics/molecular mechanics (QM/MM) strategy was further employed to probe the catalytic mechanism of the initial ring-opening step in the hydrolysis of the substrate catalyzed by NDM-1. Such theoretical studies are important because they not only can bridge the gap between experimental measurements and atomistic understanding of the enzymatic process but also may pave the way for the rational design of new antibiotics.

Methodology

Molecular docking

Glide calculations were performed with Maestro v7.5 (Schrodinger, Inc.) to obtain the starting structure [34]. Meropenem was docked into the active site of the NDM-1 enzyme with a standard protocol. Hydrogen atoms and charges of the enzyme were added during a brief relaxation performed using the Protein Preparation module in Maestro with the "Preparation and refinement" option, and a restrained partial minimization was terminated when the root-mean-square deviation (RMSD) reached the maximum value of 0.3 Å to relieve steric clashes. The grid-enclosing box was centered on the ligand and defined so as to enclose residues located within 15 Å. In the docking process, extra-precision docking was adopted to generate the minimized pose. The final docking poses between meropenem and NDM-1 were chosen based on the Glide docking scores (G-Scores) and previous studies [22, 35, 36]. The NDM-1 protein structures in models A and B were derived from the NDM-1/ampicillin complex structure published in PDB (PDB code 3Q6X) with the hydrolyzed ampicillin deleted. The enzyme structures in models C and D were derived from the same complex structure (PDB code 3Q6X) but with the oxygen atom of the hydrolyzed ampicillin coordinated to Zn2 manually changed to the oxygen atom of water.

MD simulation

MD simulations were performed on the enzyme-substrate (ES) complex obtained from molecular docking. Before simulations, the protonation states of ionizable residues were determined using the H ++ program [37], except the

D124 residue, for which two protonation states were considered. The complex was solvated into a rectangular box with a 12 Å buffer distance between the solvent box wall and the nearest solute atoms. The counterions were then added to the system to neutralize the simulation system. Finally, the whole system was subjected to energy minimization. After this step, an equilibration period of 2 ns was followed by a 30 ns production run for the ES complex. The charges of the atoms of meropenem were calculated using the RESP method [38] encoded in the AMBER suite of programs [39] at the level of HF/6-31G*. Covalent and nonbonded parameters for the meropenem atoms were derived from the general Amber force field (GAFF) [40]. The charges and force field parameters for the Zn-ligand center (two zinc ions, hydroxide, apical water and six residues coordinated to Zn1 and Zn2) were taken from previous work [32] and calculated using the MCPB approach [41].

All MD simulations were carried out using the AMBER package (version 10.0) with constant temperature and pressure and periodic boundary conditions. The Amber99SB [42–44] force field and TIP3P model [45] were used for protein and water molecules, respectively. During MD simulations, all bonds involving hydrogen atoms were constrained with the SHAKE algorithm [46], and an integration step of 2 fs was used. Electrostatic interactions were calculated using the particle-mesh Ewald method [47]. The nonbonded cutoff was set to 10 Å, and the nonbonded pairs were updated every 25 steps. Each simulation was coupled to a 300 K thermal bath at 1 atm of pressure (atm = 101.3 kPa) by applying the algorithm of Berendsen et al. [48]. The temperature and pressure coupling parameters were set at 1 ps.

QM/MM calculations

QM/MM calculations were performed using a two-layer ONIOM scheme encoded in the Gaussian03 program. The ONIOM method is a hybrid quantum chemical approach developed by Morokuma et al. that allows different levels of a theory to be applied to different parts of a molecular system [49–54]. In this approach, the molecular system under investigation is defined as two parts: The "model" system consists of the most critical elements of the system and is treated with an accurate (high-level) computational method that can describe bond breaking and formation, whereas the "real" system includes the entire system and is treated with an inexpensive (low-level) computational method which can depict the environmental effects of the molecular environment on the "model" system. The total ONIOM energy, E_{ONIOM}, is defined as follows:

$$E_{ONIOM} = E(high,\ model) + E(low,\ real) - E(low,\ model)$$

where *E(high, model)* is the energy of the model system (including the link atoms) at the high level of theory, *E(low, real)* is the energy of the real system at the low level of theory, and *E(low, model)* is the energy of the model system at the low level of theory. Thus, the ONIOM method allows one to perform a high-level calculation on a small, critical part of the molecular system and incorporate the effects of the surrounding elements at a lower level of theory to yield a consistent energy expression on the full system.

In this study, the initial coordinates for the QM/MM calculations were provided by the MD simulations. The QM region consisted of the entire substrate meropenem, the two zinc ions, the hydroxide ion, the apical water, and the side chains of the protein ligands (H120, H122, H189, D124, C208, and H250). Link hydrogen atoms [55, 56] were employed to saturate the dangling covalent bonds. The QM region was described in terms of the density functional theory with the B3LYP exchange–correlation functional and 6-31G* basis set. The remainder of the system (MM region) was treated with the AMBER Parm99SB force field. The electrostatic interactions between the QM and MM regions were calculated by an electronic embedding scheme. The partial charges of the MM region were incorporated into QM Hamiltonian, which provides a better description of the electrostatic interaction between the QM and MM regions and allows the QM wave function to be polarized. The charges for all the QM atoms were fitted to the electrostatic potential at points selected according to the Merz–Singh–Kollman scheme and calculated at the B3LYP/6-31G* level. The minimized structure optimized using the AMBER Parm99 force field was further optimized at the ONIOM (B3LYP/6-31G*: Amber) level.

Results

ES complex models

As there are two proposed substrate binding modes between B1 MBLs and substrates, this study considered both the direct and indirect binding modes. In addition, there has been controversy about the protonation states of D86 residue chelated with Zn2 in CcrA, as both ionized D86 [23, 28, 57, 58] and neutral D86 [32, 59, 60] have been proposed. Thus, as illustrated in Fig. 1, four configurations of the active site of NDM-1 interacting with meropenem β-lactam antibiotic were constructed by molecular docking (see Methodology) to represent two initial binding modes [23, 33] and two probable protonation states of the D124 residue. Models A and B, which differ only in the protonation states of D124, represent the direct binding mode in which the ES complex feature a direct substrate–metal

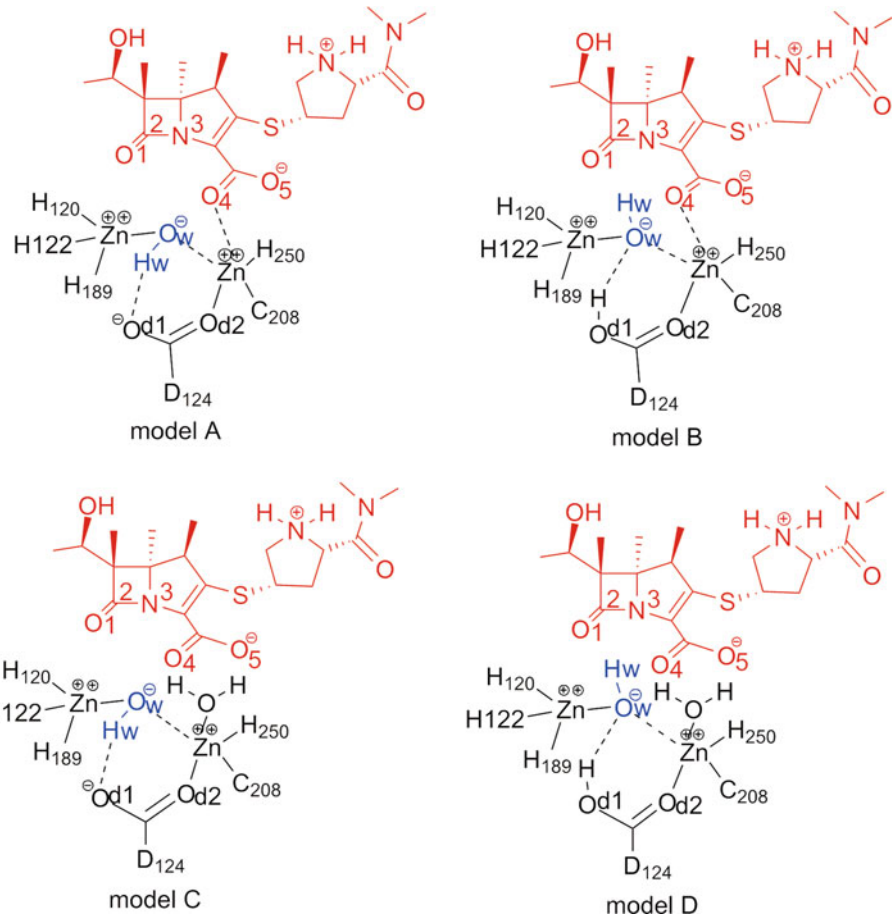

Fig. 1 Four ES models representing different binding modes and different protonation states of D124 are constructed. Model A mimics the direct binding mode in which the carboxyl group of the β-lactam antibiotic contacts Zn2 directly and D124 ionized, model B also mimics the direct binding model but with neutral D124, model C mimics the indirect binding mode in which a water ligand is coordinated to Zn2 located between the carboxyl group of the β-lactam antibiotic and Zn2 as well as with D124 ionized, and model D also mimics the indirect binding model but with neutral D124. The molecule in *red* is the substrate meropenem, and the rest represents the active site of NDM-1. Only the two zinc ions, hydroxide ion and ligands of the zinc ions of NDM-1 are shown for clarity

contact. In particular, the oxygen atoms of the carboxylate group of the β-lactam ring displace the apical water observed in the apo-enzyme, becoming one ligand of Zn2. In these two models, Zn1 is coordinated by three histidine residues (H120, H122, and H189) and a hydroxide ligand, whereas Zn2 is liganded to the hydroxide and D124, C208 and H250 residues. Models C and D correspond to the indirect binding mode in which the apical water is coordinated to Zn2 and is located between Zn2 and the substrate. Two protonation states of D124 were also considered. The four ES complex structures were used as initial structures for subsequent MD and QM/MM studies.

To investigate the stability of the active site cavity and the reaction environment, we performed 30 ns MD simulations on the four ES models. As an estimation of the structural stability of the ES complex during the MD simulations, the temporal development of weighted root-mean-square deviations (RMSD) for backbone atoms of the NDM-1 enzyme from their initial positions ($t = 0$) was calculated. Overall, the RMSD values of the four ES models (see Fig. S1 of Supplementary Material) remained between 0.5 and 2 Å. The steady RMSD value for the atoms of the ES complex indicated that the systems were well equilibrated and that catalytic cavity of each model was relatively stable during the MD simulation, thus rendering the MD trajectories of the four ES complex models reliable for post analysis.

QM/MM calculations on the catalytic reaction step: nucleophilic displacement

Sampling from MD trajectories

QM/MM calculations were performed on each ES model to further explore the detail mechanism of the nucleophilic displacement step in the catalytic reaction. The starting structures for QM/MM calculations were sampled from the MD trajectories. It should be noted that a proper sampling methodology is pivotal to the reliability of QM/MM calculations. Zhang et al. [17] determined the crystal structure of NDM-1 in complex with a hydrolyzed ampicillin (PDB code 3Q6X) and proposed that the binding between the NDM-1 active site and its substrates involved several critical interactions. Specifically, the carboxylate group on the β-lactam antibiotic coordinated to Zn2 through one oxygen atom and formed a salt bridge with the Nζ atom of K211 through the other oxygen atom. The oxygen atom of the carbonyl group of the β-lactam ring hydrogen bonded to the Nδ2 atom of N220. Together with

other reported studies on direct substrate binding modes of B1 subclass MBLs, the sampling principles for models A and B can be summarized as follows: (1) the oxygen atom of the carbonyl group of the β-lactam ring should orientate to Zn1 and form a hydrogen bond with the Nδ2 atom of N220 and (2) the oxygen atoms of the carboxylate group of the β-lactam antibiotic should coordinate to Zn2 and form a salt bridge with the Nζ atom of K211. Furthermore, taking the extent of RMSD fluctuations into account, structure snapshots at 16.2 and 16 ns were extracted from the MD trajectories of models A and B, respectively, and selected as the initial structures (Supplementary Material Fig. S2) for subsequent QM/MM studies. As for the indirect binding mode, a water ligand was located between Zn2 and the carboxylate group of the β-lactam ring, so the sampling principle for models C and D was that the oxygen atom of the carbonyl group of the β-lactam ring should orientate to Zn1 and form a hydrogen bond with the Nδ2 atom of N220 residue. In addition, considering RMSD fluctuations, snapshots at 14.2 and 12 ns were extracted from the MD trajectories of models C and D and selected as the initial structures (Supplementary Material Fig. S2) for QM/MM calculations.

Potential energy profile of the four models

To study the nucleophilic displacement step of the β-lactam antibiotic catalyzed by NDM-1, we concentrated on the putative reaction coordinates (RCs) associated with the hydroxide nucleophile attack to the lactam carbonyl carbon (C2) in the nucleophilic addition. R(O_w–C2) (the distance between O_w at hydroxide and C2 at meropenem) was designed as the RC during the ring opening step of the reaction. Systematically pulling the catalytic hydroxide oxygen atom (O_w) toward the β-lactam carbonyl carbon (C2) (at 0.1 Å intervals), gave one-dimensional potential energy profile. As illustrated in Fig. 2, the one-dimensional potential energy profiles of the four ES models were calculated by the employing the QM/MM approach. According to the potential energy profiles calculated by QM/MM method, the potential energy barrier for the nucleophilic addition in models B and D was significantly higher than that in model A, suggesting that ionized D124 was more effective in catalyzing ring opening reaction step than the neutral one. On the other hand, in model A, which contained an ionized D124 but no chelated water in Zn2, the C2–N3 bond automatically broke when the R(O_w–C2) reached 1.28 Å. As for model C, which also contained an ionized D124 and chelated water in Zn2, the C2–N3 bond was still intact when the R(O_w–C2) reached 1.31 Å. When R(O_w–C2) was further shortened from 1.31 to 1.28 Å at the intervals of 0.01 Å in model C, the C2–N3 bond eventually broke and one of the protons of the apical water molecules coordinated to Zn2 transferred to N3 simultaneously.

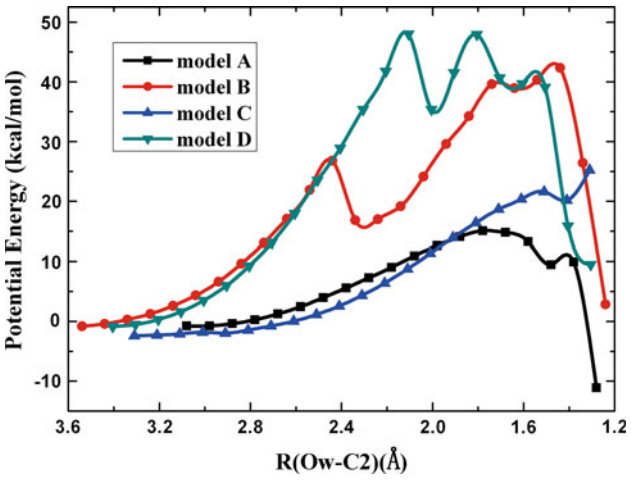

Fig. 2 One-dimensional potential energy profiles of the four models obtained by defining the distance of R(O_w–C2) as the RC

However, the potential energy barrier (not shown) in model C was higher than that in model A and these results are not consistent with the experimental data [61]. Thus, based on the above described analysis, model A may represent the most probable initial structure for the catalytic reaction.

In the process of pulling the hydroxide (Ow) towards the lactam carbonyl carbon (C2), the C2–N3 bond length was also undergoing large changes. In order to study the detailed energy profile around the transition state (TS) and take the change of C2–N3 bond length into consideration, we obtained a contour plot of two-dimensional QM/MM potential energy surface (PES) of the most favorable reaction mechanism (model A) by systematically lengthening the distances of R(O_w–C2) from 2.08 to 1.28 Å and shortening the distance of R(C2–N3) from 1.45 to 2.65 Å simultaneously (Fig. 3c). According to the PES, more precise coordinates of TS1, TI and TS2 can be identified directly. Specifically, TS1 is located at R(O_w–C2) = 1.72 Å, R(C2–N3) = 1.58 Å; TI is located at R(O_w–C2) = 1.45 Å, R(C2–N3) = 1.62 Å, and TS2 is located at R(O_w–C2) = 1.38 Å, R(C2–N3) = 1.72 Å, respectively. These coordinates are slightly different (within 0.1 Å) from the coordinates of TS1, TI and TS2 calculated by defining only one reaction coordinates. Although the potential energy of TS1 obtained from two-dimensional potential energy surface is about 3 kcal/mol lower than that by using only one reaction coordinate, which may result from a more precise TS1 coordinate derived from the two-dimensional surface. However, the potential energy of TI and TS2 calculated using one or two reaction coordinates are very similar (Fig. 3c).

Further analysis of the intermediate structures along the RCs in model A revealed that the nucleophilic attack of the lactam carbonyl carbon (C2) by the bridging hydroxide (O_w) arouses a series of geometric changes in both the

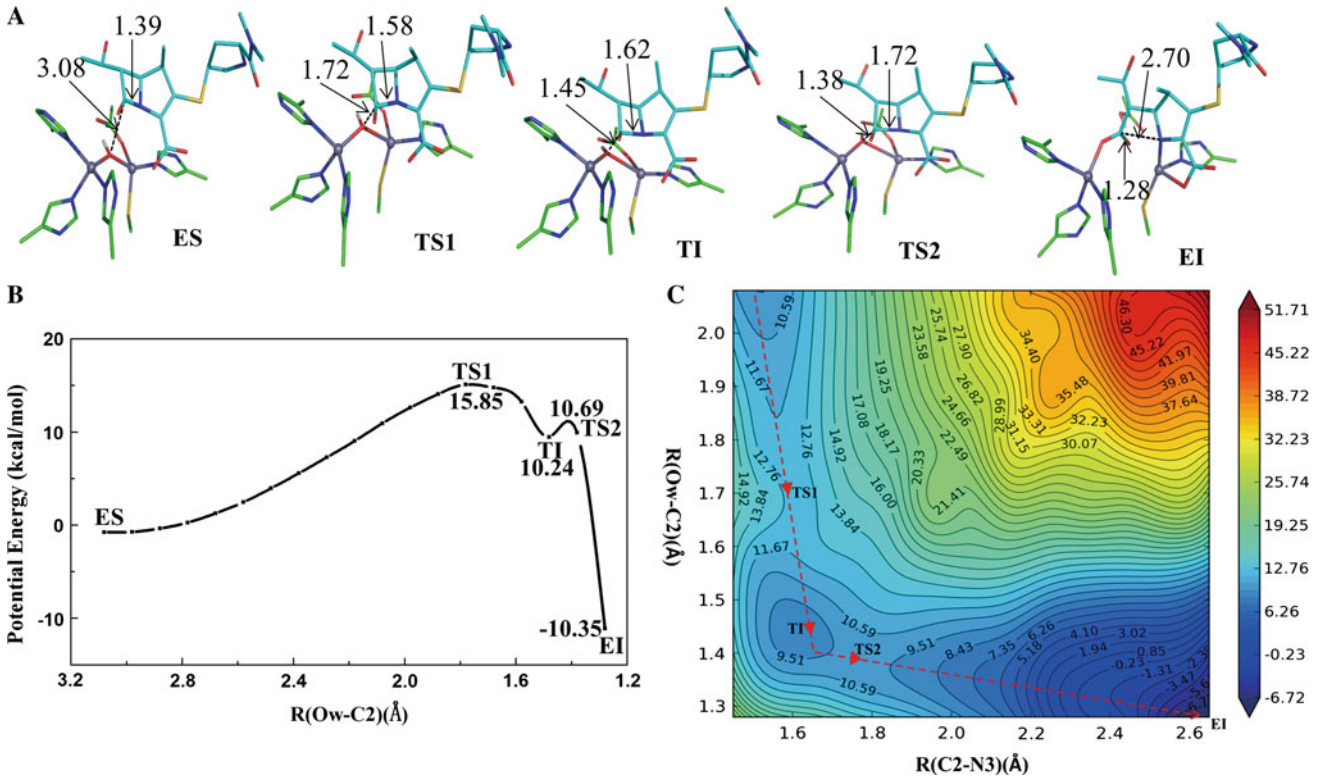

Fig. 3 Potential energy profile for model A and snapshots of the QM/MM stationary points along the reaction path for the hydrolysis of meropenem catalyzed by NDM-1. **a** The QM/MM optimized structures of the enzyme-substrate (ES), transition states (TS1, TS2), tetrahedral intermediate (TI), and enzyme-intermediate (EI). For clarity, only the structures in the QM region are shown, and all the hydrogen atoms are omitted except for that involved in the proton transfer. The distances of O_w–C2 and C2–N3 are labeled. The distances are given in Angstrom. **b** One-dimensional potential energy profile of model A. **c** Contour plot of the potential energy surface (PES) obtained by defining R(O_w–C2) and R(C2–N3) as reaction coordinates

enzyme and the substrate. In particular, an enzyme–intermediate (EI) complex featuring a cleaved lactam amide C2–N3 bond, and two transition states (TSs) between ES and EI were found in our QM/MM simulations. The first TS (TS1) is characterized largely by the shortening of the O_w–C2 distance, which changed from 3.08 Å in ES to 1.72 Å in TS1. On the other hand, the second TS (TS2) mainly involves the cleavage of the amide bond, as evidenced by the elongation of the C2–N3 distance from 1.72 Å in TS2 to 2.70 Å in EI. The relative geometries of these stationary states are illustrated in Fig. 3a. Interestingly, accompanied by the cleavage of C2–N3, the proton of the hydroxide transferred to O_{d1} of D124 simultaneously (Supplementary Material Fig. S3), which is in line with the mechanistic proposal for the CcrA B1 MBL suggested by Park et al. [23]. The proton transfers to O_{d1} of D124 made D124 become weakly liganded to Zn2, as evidenced by the longer distance between Zn2 and O_{d2} shown in Table 1. All the catalytic features, including two TSs, proton transfer, and weaker coordination of D124 to Zn2, could also be found in the catalytic mechanism of L1 MBL proposed by Xu et al. [26]. Thus, we suggest that NDM-1 may adopt a catalytic mechanism very similar to that of L1 MBL. In addition, as shown in Fig. 3b, the potential energy barrier was determined to be 15.85 kcal/mol, which is consistent with the fact that meropenem is readily hydrolyzed by NDM-1.

Discussion

Proposed catalytic mechanism of the nucleophilic displacement

The hydrolysis mechanism of meropenem catalyzed by NDM-1 is shown in Fig. 4. Specifically, the reaction is started by the zinc-bridging hydroxide attacking the carbonyl carbon of meropenem as shown in the ES complex and the addition of the nucleophilic hydroxide to C2 leads to cleavage of the lactam C2–N3 bond, possibly via a tetrahedral intermediate flanked by two TSs TS1 and TS2. The resulting anionic nitrogen leaving group is then stabilized by the Zn2 ion as depicted in the EI complex. The stabilization of the nitrogen anionic intermediate by Zn2 is quite consistent with previous experimental observations

Table 1 Selected geometry parameters for stationary points along the reaction path for the hydrolysis of meropenem catalyzed by NDM-1

	Bond distance (Å)				
	ES	TS1	TI	TS2	EI
O_w···C2	3.08	1.72	1.45	1.38	1.28
C2···N3	1.39	1.58	1.62	1.72	2.70
O1···C2	1.21	1.24	1.29	1.31	1.28
H_w···O_w	0.99	1.02	1.05	1.07	1.68
Zn2···N3	3.43	2.53	2.18	2.14	1.96
Zn2···O4	2.23	2.13	2.29	2.28	2.15
Zn2···O_w	1.96	2.26	2.52	2.66	2.40
Zn1···O1	3.15	2.94	2.12	2.06	1.90
Zn1···O_w	1.86	1.93	2.07	2.13	3.52
H_w···O_{d1}(D124)	1.71	1.62	1.44	1.39	1.00
Zn1···N_ε(H120)	2.04	2.05	2.11	2.11	2.00
Zn1···N_δ(H122)	2.05	2.05	2.06	2.07	2.04
Zn1···N_ε(H189)	2.06	1.93	2.06	2.07	2.03
Zn2···O_{d2}(D124)	2.10	2.06	2.12	2.13	4.75
Zn2···S(C208)	2.36	2.37	2.35	2.34	2.32
Zn2···N_ε(H250)	2.14	2.15	2.10	2.09	2.12
Zn1···Zn2	3.60	3.79	4.06	4.17	4.49

[61] and similar to the catalytic mechanism of other MBLs [23, 26, 57, 62].

According to the fluctuations of bond lengths shown in Table 1, as the nucleophilic agent hydroxide attacked to the carbonyl carbon of meropenem, the distance between the two zinc ions increased from 3.60 Å in ES to 4.49 Å in EI. This phenomenon may help explain the discrepancy in the Zn–Zn distance in different crystal structures of NDM-1. The Zn–Zn distance varies from 3.2 to 4.59 Å in crystal structures, and mutagenesis studies on B1 MBLs (BcII) revealed that mutations leading to an increase in the Zn–Zn distance would damage the catalytic activity of the enzyme [63]. Thus, we suggest that the distance between the zinc ions should be approximately 3.6 Å before the enzymatic reaction, which is in line with the distance of 3.58 Å obtained by QM/MM MD simulations [64], and that the distance of 4.59 Å in crystal structure 3Q6X may represent a special state relative to the product release.

The molecular basis for NDM-1 hydrolyzing meropenem was also probed by analyzing the hydrogen-bond and hydrophobic interactions in the active site of model A. In all, the hydrogen-bonds between Nζ atom of K211 and the O4, O5 atoms of meropenem were conserved during the 30 ns MD simulation as indicated by their occupancies

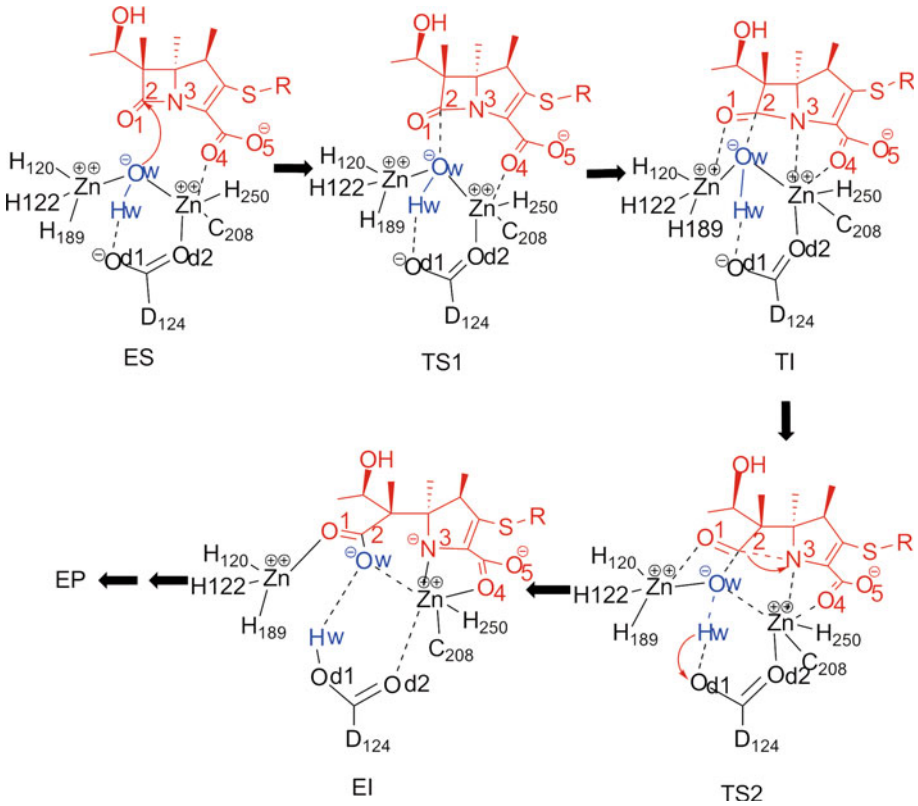

Fig. 4 Proposed mechanism for the nucleophilic displacement step in meropenem hydrolysis catalyzed by NDM-1. *TI* tetrahedral intermediate, *EP* enzyme product. The molecule in *red* is the meropenem, and the other molecules represent the active site of NDM-1

Table 2 Hydrogen bonds in the ES complex and their occupancies in the 30-ns MD simulation of model A

H-bond donor	H-bond acceptor	H-bond occupancy (%)
K211:NZ	Meropenem:O5	92.20
K211:NZ	Meropenem:O4	61.06

Only the H-bond occupancies >50 % were shown

(see Table 2), which further indicated the pivotal role of K211 in maintaining the proper orientation of substrates in the binding pocket, thus facilitating the catalytic reaction. The importance of K211 has been verified by mutagenesis studies reporting that K211A and K211E mutations in NDM-1 completely abolished its catalytic activity [36]. As another driving force in the substrate binding process, hydrophobic interactions also play an important role in stabilizing the substrate in the NDM-1 active site. Details of the hydrophobic interactions between meropenem and NDM-1 are plotted in Supplementary Material Fig. S4. As shown in Fig. S4, M67, F70, and V73 residues in loop L1 (residues 65–73) as well as K211, S217, G219, and N220 residues in loop L2 (residues 205–225) had conserved hydrophobic interactions with meropenem. Taken together, the consistency between simulation results and experimental data demonstrated that the MD simulation on the NDM-1/meropenem substrate complex is reasonable.

The oxygen atom (O_{d1}) of D124 notably forms a strong hydrogen bond with the hydroxide in model A, which could significantly increase the nucleophilic reactivity of the hydroxide. However, in model B, D124 is protonated, and the proton of O_{d1} establishes a hydrogen bond with the O_w of the hydroxide, which negatively affects the nucleophilic reactivity of the hydroxide. In addition, the ionized D124 could act as a proton receptor when the nucleophilic agent hydroxide attacks the carbonyl carbon (C2), thus further lowering the potential energy barrier of the nucleophilic displacement reaction. While in models C and D, in which a water molecule is chelated with Zn2 and located between Zn2 and meropenem, the carboxylate of meropenem could not form the conserved hydrogen bond with K211 side chains, thus possibly leading to the instability of substrates in the NDM-1 pocket.

Conclusions

Although NDM-1 has the ability to hydrolyze almost all clinically used β-lactam antibiotics, its catalytic mechanism remains unclear and effective inhibitors of NDM-1 have yet to be identified. In this study, the hydrolysis of meropenem catalyzed by NDM-1 was studied by QM/MM simulation. The results showed that the binding mode between NDM-1 and meropenem features a direct substrate–metal contact in which the carboxylate group of meropenem chelates with the active site of Zn2 directly. The calculation results also showed that ionized D124, rather than neutral D124 could facilitate the cleavage of the substrate C–N bond. The EI obtained by the QM/MM method, in which the anionic nitrogen stabilized by Zn2 is quite consistent with the experimental results, further supports the catalytic mechanism we proposed. That is, the nucleophilic attack of the carbonyl carbon (C2) by the hydroxide results in an EI complex product, possibly via two TSs, TS1 and TS2, which correspond to a nucleophilic addition barrier and a nucleophilic elimination barrier, respectively. Our study provides a detailed mechanism for the nucleophilic displacement step of catalytic hydrolysis of meropenem by NDM-1, elucidates the molecular basis for this reaction, and may shed light on the discovery of novel mechanism-based inhibitors of NDM-1.

Acknowledgments This work was support by grants from National High Technology Research and Development Program of China (2012AA020302), National Natural Science Foundation of China (20972174, 91029704, 21073034, 21210003 and 21021063), the Key Project of Chinese National Programs for Fundamental Research and Development (2009CB918502), the Natural Science Foundation of the Fujian Province (2010J05023), the Guangdong S&T Dept. (2010A030100006) and the "Key New Drug Creation and Manufacturing Program" (2013ZX09507-004).

References

1. Drawz SM, Bonomo RA (2010) Three decades of beta-lactamase inhibitors. Clin Microbiol Rev 23(1):160–201. doi:10.1128/CMR.00037-09
2. Hall BG, Barlow M (2005) Revised Ambler classification of {beta}-lactamases. J Antimicrob Chemother 55(6):1050–1051. doi:10.1093/jac/dki130
3. Bush K (1998) Metallo-beta-lactamases: a class apart. Clin Infect Dis 27(Suppl 1):S48–S53
4. Bush K, Jacoby GA (2010) Updated functional classification of beta-lactamases. Antimicrob Agents Chemother 54(3):969–976. doi:10.1128/AAC.01009-09
5. Crowder MW, Spencer J, Vila AJ (2006) Metallo-beta-lactamases: novel weaponry for antibiotic resistance in bacteria. Acc Chem Res 39(10):721–728. doi:10.1021/ar0400241
6. Galleni M, Lamotte-Brasseur J, Rossolini GM, Spencer J, Dideberg O, Frere JM (2001) Standard numbering scheme for class B beta-lactamases. Antimicrob Agents Chemother 45(3):660–663. doi:10.1128/AAC.45.3.660-663.2001
7. Papp-Wallace KM, Endimiani A, Taracila MA, Bonomo RA (2011) Carbapenems: past, present, and future. Antimicrob Agents Chemother 55(11):4943–4960. doi:10.1128/AAC.00296-11
8. Perez-Llarena FJ, Bou G (2009) beta-Lactamase inhibitors: the story so far. Curr Med Chem 16(28):3740–3765
9. Yong D, Toleman MA, Giske CG, Cho HS, Sundman K, Lee K, Walsh TR (2009) Characterization of a new metallo-beta-lactamase gene, bla(NDM-1), and a novel erythromycin esterase gene carried on a unique genetic structure in Klebsiella pneumoniae

sequence type 14 from India. Antimicrob Agents Chemother 53(12):5046–5054. doi:10.1128/Aac.00774-09
10. Kumarasamy KK, Toleman MA, Walsh TR, Bagaria J, Butt F, Balakrishnan R, Chaudhary U, Doumith M, Giske CG, Irfan S, Krishnan P, Kumar AV, Maharjan S, Mushtaq S, Noorie T, Paterson DL, Pearson A, Perry C, Pike R, Rao B, Ray U, Sarma JB, Sharma M, Sheridan E, Thirunarayan MA, Turton J, Upadhyay S, Warner M, Welfare W, Livermore DM, Woodford N (2010) Emergence of a new antibiotic resistance mechanism in India, Pakistan, and the UK: a molecular, biological, and epidemiological study. Lancet Infect Dis 10(9):597–602. doi:10.1016/S1473-3099(10)70143-2
11. Nordmann P, Poirel L, Walsh TR, Livermore DM (2011) The emerging NDM carbapenemases. Trends Microbiol 19(12):588–595. doi:10.1016/j.tim.2011.09.005
12. Poirel L, Dortet L, Bernabeu S, Nordmann P (2011) Genetic features of blaNDM-1-positive Enterobacteriaceae. Antimicrob Agents Chemother 55(11):5403–5407. doi:10.1128/AAC.00585-11
13. Livermore DM, Mushtaq S, Warner M, Zhang JC, Maharjan S, Doumith M, Woodford N (2011) Activity of aminoglycosides, including ACHN-490, against carbapenem-resistant Enterobacteriaceae isolates. J Antimicrob Chemother 66(1):48–53. doi:10.1093/jac/dkq408
14. Nordmann P, Naas T, Poirel L (2011) Global spread of carbapenemase-producing enterobacteriaceae. Emerging Infect Dis 17(10):1791–1798. doi:10.3201/eid1710.110655
15. Walsh TR, Weeks J, Livermore DM, Toleman MA (2011) Dissemination of NDM-1 positive bacteria in the New Delhi environment and its implications for human health: an environmental point prevalence study. Lancet Infect Dis 11(5):355–362. doi:10.1016/S1473-3099(11)70059-7
16. Hishinuma A, Ishida T (2012) New Delhi metallo -beta-lactamase-1 (NDM-1) producing bacteria. Nippon Rinsho 70(2):262–266
17. Zhang H, Hao Q (2011) Crystal structure of NDM-1 reveals a common beta-lactam hydrolysis mechanism. FASEB J 25(8):2574–2582. doi:10.1096/fj.11-184036
18. Kim Y, Tesar C, Mire J, Jedrzejczak R, Binkowski A, Babnigg G, Sacchettini J, Joachimiak A (2011) Structure of apo- and monometalated forms of NDM-1–a highly potent carbapenem-hydrolyzing metallo-beta-lactamase. PLoS One 6(9):e24621. doi:10.1371/journal.pone.0024621
19. Guo Y, Wang J, Niu G, Shui W, Sun Y, Zhou H, Zhang Y, Yang C, Lou Z, Rao Z (2011) A structural view of the antibiotic degradation enzyme NDM-1 from a superbug. Protein Cell 2(5):384–394. doi:10.1007/s13238-011-1055-9
20. Green VL, Verma A, Owens RJ, Phillips SE, Carr SB (2011) Structure of New Delhi metallo-beta-lactamase 1 (NDM-1). Acta Crystallogr, Sect F: Struct Biol Cryst Commun 67(Pt 10):1160–1164. doi:10.1107/S1744309111029654
21. King D, Strynadka N (2011) Crystal structure of New Delhi metallo-beta-lactamase reveals molecular basis for antibiotic resistance. Protein Sci 20(9):1484–1491. doi:10.1002/pro.697
22. Wang Z, Fast W, Valentine AM, Benkovic SJ (1999) Metallo-beta-lactamase: structure and mechanism. Curr Opin Chem Biol 3(5):614–622
23. Park H, Brothers EN, Merz KM Jr (2005) Hybrid QM/MM and DFT investigations of the catalytic mechanism and inhibition of the dinuclear zinc metallo-beta-lactamase CcrA from Bacteroides fragilis. J Am Chem Soc 127(12):4232–4241. doi:10.1021/ja042607b
24. Simona F, Magistrato A, Dal Peraro M, Cavalli A, Vila AJ, Carloni P (2009) Common mechanistic features among metallo-beta-lactamases: a computational study of Aeromonas hydrophila CphA enzyme. J Biol Chem 284(41):28164–28171. doi:10.1074/jbc.M109.049502
25. Garau G, Bebrone C, Anne C, Galleni M, Frere JM, Dideberg O (2005) A metallo-beta-lactamase enzyme in action: crystal structures of the monozinc carbapenemase CphA and its complex with biapenem. J Mol Biol 345(4):785–795. doi:10.1016/j.jmb.2004.10.070
26. Xu D, Guo H, Cui Q (2007) Antibiotic deactivation by a dizinc beta-lactamase: mechanistic insights from QM/MM and DFT studies. J Am Chem Soc 129(35):10814–10822. doi:10.1021/ja072532m
27. Sharma NP, Hajdin C, Chandrasekar S, Bennett B, Yang KW, Crowder MW (2006) Mechanistic studies on the mononuclear ZnII-containing metallo-beta-lactamase ImiS from Aeromonas sobria. Biochemistry 45(35):10729–10738. doi:10.1021/bi060893t
28. Yanchak MP, Taylor RA, Crowder MW (2000) Mutational analysis of metallo-beta-lactamase CcrA from Bacteroides fragilis. Biochemistry 39(37):11330–11339
29. Oelschlaeger P, Schmid RD, Pleiss J (2003) Insight into the mechanism of the IMP-1 metallo-beta-lactamase by molecular dynamics simulations. Protein Eng 16(5):341–350. doi:10.1093/protein/gzg049
30. Carenbauer AL, Garrity JD, Periyannan G, Yates RB, Crowder MW (2002) Probing substrate binding to metallo-beta-lactamase L1 from Stenotrophomonas maltophilia by using site-directed mutagenesis. BMC Biochem 3:4
31. Wu SS, Xu DG, Guo H (2010) QM/MM studies of monozinc beta-lactamase CphA suggest that the crystal structure of an enzyme-intermediate complex represents a minor pathway. J Am Chem Soc 132(51):17986–17988. doi:10.1021/Ja104241g
32. Suarez D, Brothers EN, Merz KM (2002) Insights into the structure and dynamics of the dinuclear zinc beta-lactamase site from Bacteroides fragilis. Biochemistry 41(21):6615–6630. doi:10.1021/Bi0121860
33. Dal Peraro M, Vila AJ, Carloni P, Klein ML (2007) Role of zinc content on the catalytic efficiency of B1 metallo beta-lactamases. J Am Chem Soc 129(10):2808–2816. doi:10.1021/Ja0657556
34. Friesner RA, Banks JL, Murphy RB, Halgren TA, Klicic JJ, Mainz DT, Repasky MP, Knoll EH, Shelley M, Perry JK, Shaw DE, Francis P, Shenkin PS (2004) Glide: a new approach for rapid, accurate docking and scoring. 1. Method and assessment of docking accuracy. J Med Chem 47(7):1739–1749. doi:10.1021/jm0306430
35. Bounaga S, Laws AP, Galleni M, Page MI (1998) The mechanism of catalysis and the inhibition of the Bacillus cereus zinc-dependent beta-lactamase. Biochem J 331(Pt 3):703–711
36. Liang Z, Li L, Wang Y, Chen L, Kong X, Hong Y, Lan L, Zheng M, Guang-Yang C, Liu H, Shen X, Luo C, Li KK, Chen K, Jiang H (2011) Molecular basis of NDM-1, a new antibiotic resistance determinant. PLoS One 6(8):e23606. doi:10.1371/journal.pone.0023606
37. Gordon JC, Myers JB, Folta T, Shoja V, Heath LS, Onufriev A (2005) H++: a server for estimating pKas and adding missing hydrogens to macromolecules. Nucleic Acids Res 33(Web Server issue):W368–W371. doi:10.1093/nar/gki464
38. Bayly CI, Cieplak P, Cornell WD, Kollman PA (1993) A well-behaved electrostatic potential based method using charge restraints for deriving atomic charges—the resp model. J Phys Chem 97(40):10269–10280
39. Case DA, Cheatham TE, Darden T, Gohlke H, Luo R, Merz KM, Onufriev A, Simmerling C, Wang B, Woods RJ (2005) The Amber biomolecular simulation programs. J Comput Chem 26(16):1668–1688. doi:10.1002/Jcc.20290
40. Wang J, Wolf RM, Caldwell JW, Kollman PA, Case DA (2004) Development and testing of a general amber force field. J Comput Chem 25(9):1157–1174. doi:10.1002/jcc.20035
41. Peters MB, Yang Y, Wang B, Fusti-Molnar L, Weaver MN, Merz KM (2010) Structural Survey Of Zinc-Containing Proteins And Development Of The ZINC AMBER Force Field (ZAFF). J Chem Theory Comput 6(9):2935–2947. doi:10.1021/Ct1002626
42. Cornell WD, Cieplak P, Bayly CI, Gould IR, Merz KM, Ferguson DM, Spellmeyer DC, Fox T, Caldwell JW, Kollman PA (1995) A second generation force field for the simulation of proteins,

nucleic acids, and organic molecules. J Am Chem Soc 117(19): 5179–5197
43. Wang JM, Cieplak P, Kollman PA (2000) How well does a restrained electrostatic potential (RESP) model perform in calculating conformational energies of organic and biological molecules? J Comput Chem 21(12):1049–1074
44. Hornak V, Abel R, Okur A, Strockbine B, Roitberg A, Simmerling C (2006) Comparison of multiple amber force fields and development of improved protein backbone parameters. Proteins Struct Funct Bioinf 65(3):712–725. doi:10.1002/Prot.21123
45. Jorgensen WL, Chandrasekhar J, Madura JD, Impey RW, Klein ML (1983) Comparison of simple potential functions for simulating liquid water. J Chem Phys 79(2):926–935
46. Ryckaert JP, Ciccotti G, Berendsen HJC (1977) Numerical-integration of cartesian equations of motion of a system with constraints—molecular-dynamics of N-Alkanes. J Comput Phys 23(3):327–341
47. Darden T, York D, Pedersen L (1993) Particle mesh Ewald—an N.Log(N) method for Ewald sums in large systems. J Chem Phys 98(12):10089–10092
48. Berendsen HJC, Postma JPM, Vangunsteren WF, Dinola A, Haak JR (1984) Molecular-dynamics with coupling to an external bath. J Chem Phys 81(8):3684–3690
49. Maseras F, Morokuma K (1995) Imomm—a new integrated ab-initio plus molecular mechanics geometry optimization scheme of equilibrium structures and transition-states. J Comput Chem 16(9):1170–1179
50. Svensson M, Humbel S, Morokuma K (1996) Energetics using the single point IMOMO (integrated molecular orbital plus molecular orbital) calculations: choices of computational levels and model system. J Chem Phys 105(9):3654–3661
51. Dapprich S, Komaromi I, Byun KS, Morokuma K, Frisch MJ (1999) A new ONIOM implementation in Gaussian98. Part I. The calculation of energies, gradients, vibrational frequencies and electric field derivatives. J Mol Struct Theochem 461:1–21
52. Vreven T, Morokuma K (2000) On the application of the IMOMO (integrated molecular orbital plus molecular orbital) method. J Comput Chem 21(16):1419–1432
53. Vreven T, Mennucci B, da Silva CO, Morokuma K, Tomasi J (2001) The ONIOM-PCM method: combining the hybrid molecular orbital method and the polarizable continuum model for solvation. Application to the geometry and properties of a merocyanine in solution. J Chem Phys 115(1):62–72
54. Vreven T, Morokuma K, Farkas O, Schlegel HB, Frisch MJ (2003) Geometry optimization with QM/MM, ONIOM, and other combined methods. I. Microiterations and constraints. J Comput Chem 24(6):760–769. doi:10.1002/Jcc.10156
55. Field MJ, Bash PA, Karplus M (1990) A combined quantum-mechanical and molecular mechanical potential for molecular-dynamics simulations. J Comput Chem 11(6):700–733
56. Singh UC, Kollman PA (1986) A combined abinitio quantum-mechanical and molecular mechanical method for carrying out simulations on complex molecular-systems—applications to the Ch3cl + Cl− exchange-reaction and gas-phase protonation of polyethers. J Comput Chem 7(6):718–730
57. Wang Z, Fast W, Benkovic SJ (1999) On the mechanism of the metallo-beta-lactamase from Bacteroides fragilis. Biochemistry 38(31):10013–10023. doi:10.1021/bi990356r
58. Dal Peraro M, Vila AJ, Carloni P (2003) Protonation state of Asp120 in the binuclear active site of the metallo-beta-lactamase from Bacteroides fragilis. Inorg Chem 42(14):4245–4247. doi:10.1021/ic026059j
59. Gilson HSR, Krauss M (1999) Structure and spectroscopy of metallo-lactamase active sites. J Am Chem Soc 121(30): 6984–6989
60. Diaz N, Suarez D, Merz KMM (2000) Zinc metallo-beta-lactamase from Bacteroides fragilis: a quantum chemical study on model systems of the active site. J Am Chem Soc 122(17): 4197–4208
61. Yang H, Aitha M, Hetrick AM, Richmond TK, Tierney DL, Crowder MW (2012) Mechanistic and spectroscopic studies of metallo-beta-lactamase NDM-1. Biochemistry 51(18):3839–3847. doi:10.1021/bi300056y
62. Kaminskaia NV, Spingler B, Lippard SJ (2001) Intermediate in beta-lactam hydrolysis catalyzed by a dinuclear zinc(II) complex: relevance to the mechanism of metallo-beta-lactamase. J Am Chem Soc 123(27):6555–6563
63. Gonzalez JM, Medrano Martin FJ, Costello AL, Tierney DL, Vila AJ (2007) The Zn2 position in metallo-beta-lactamases is critical for activity: a study on chimeric metal sites on a conserved protein scaffold. J Mol Biol 373(5):1141–1156. doi:10.1016/j.jmb.2007.08.031
64. Thomas PW, Zheng M, Wu S, Guo H, Liu D, Xu D, Fast W (2011) Characterization of purified New Delhi metallo-beta-lactamase-1. Biochemistry 50(46):10102–10113. doi:10.1021/bi201449r